iScience

CellPress

Article

2D Graphdiyne Oxide Serves as a Superior New Generation of Antibacterial Agents

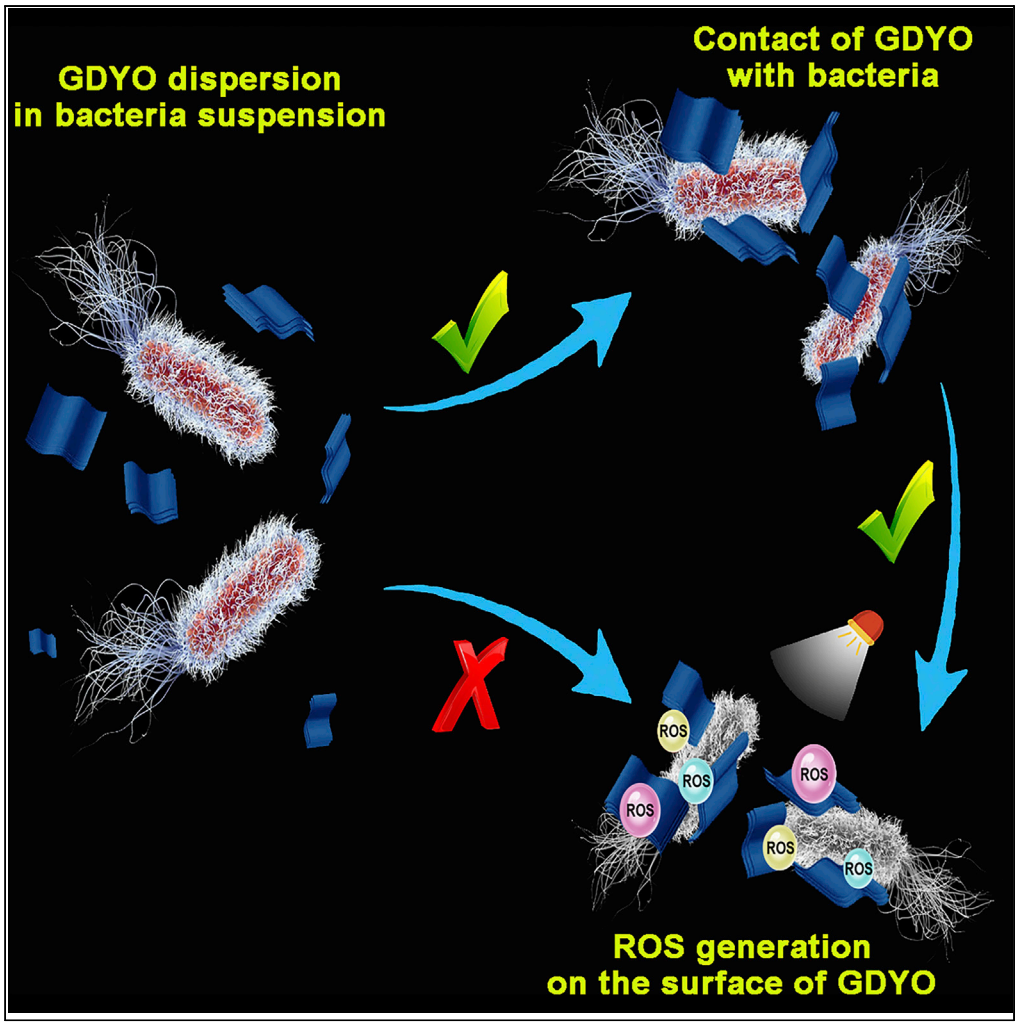

Yana Zhang, Wenxin Liu, Yongjun Li, Ying-Wei Yang, Alideertu Dong, Yuliang Li

liyj@iccas.ac.cn (Y.L.)
ywyang@jlu.edu.cn (Y.-W.Y.)
dongali@imu.edu.cn (A.D.)

HIGHLIGHTS

We report for the first time on the antibacterial behaviors of GDY and GDYO

Surface of GDY was modified with hydrophilic functional groups

Surface oxidation endows inert GDY with superior antibacterial capability

GDYO shows ROS-dependent antibacterial action after direct contact with bacteria

Zhang et al., iScience *19*, 662–675
September 27, 2019
https://doi.org/10.1016/j.isci.2019.08.019

iScience

CellPress

Article

2D Graphdiyne Oxide Serves as a Superior New Generation of Antibacterial Agents

Yana Zhang,[1,5] Wenxin Liu,[1,5] Yongjun Li,[2,*] Ying-Wei Yang,[3,4,*] Alideertu Dong,[1,5,6,*] and Yuliang Li[2]

SUMMARY

Graphdiyne (GDY) as an emerging 2D carbon-network nanomaterial possesses many fascinating properties that lead to numerous exciting applications, but the use of GDY and its derivatives in the antibacterial field has not yet been discovered. In this study, we first report on the use and evaluation of GDY and graphdiyne oxide (GDYO) as antibacterial agents and propose the antibacterial mechanisms of GDY-based nanomaterials. GDYO has been synthesized via the surface oxidation of GDY, and the antibacterial activity of GDYO has been compared with that of GDY through a series of antibacterial tests. Surprisingly, surface oxidation endowed inert GDY with superior antibacterial capability against two representative bacterial models: *Escherichia coli* and *Staphylococcus aureus*. Antibacterial mechanism experiments disclose that the antibacterial function of GDYO is a result of reactive oxygen species-dependent oxidation stress when a dispersed GDYO suspension has a direct contact with bacteria especially under visible light irradiation.

INTRODUCTION

Bacterial infections pose an unprecedented global challenge to public health, especially with the emergence of antibiotic-resistant pathogens that have developed through the overuse or misuse of antibiotics (Simpson et al., 2009; Han et al., 2011; Chambers and DeLeo, 2009; Rodriguez et al., 2014; Wellington et al., 2013). The continuing emergence and global spread of antibiotic-resistant bacterial strains have generated great interest, from bench researchers in academic laboratories to clinical trials to explore new antibacterial agents that act differently from traditional antibiotics to combat harmful pathogen-associated diseases (Li et al., 2018a; Bunders et al., 2011; Huang et al., 2015a; Sikandar et al., 2018). Compared with traditional antibiotics, antibacterial nanomaterials are not prone to generate bacterial resistance because they not only act through multiple antibacterial mechanisms simultaneously but also have good membrane permeability owing to their small sizes (Li et al., 2018b; Hemeg, 2017; Rigo et al., 2018). To date, various advanced nanomaterials—including metals and metal oxides, MoS_2, MXenes, and carbon nanomaterials, among others—have demonstrated great potential for managing bacterial infections (Tang and Zheng, 2018; Djurišić et al., 2014; Yang et al., 2014; Rasool et al., 2016; Lu et al., 2017). Of the antibacterial nanomaterials that effectively kill pathogenic bacteria, carbon nanomaterials (e.g., carbon nanotubes, graphene, graphene oxide [GO]) capable of controlling and combating bacterial infections have become some of the most popular, especially GO (Palmieri et al., 2017a, 2017b; Grace et al., 2015; Hegab et al., 2016). However, a systematic and comprehensive survey of the literature determined that these carbon nanomaterials cannot generate enough reactive oxygen species (ROS) to fight pathogenic bacteria because during the photocatalytic sterilization process, the requisite electron-hole pairs do not form efficiently enough (Chen et al., 2014a; Tu et al., 2013; Ji et al., 2016).

As graphdiyne (GDY) was first synthesized in 2010 as a new subcategory of 2D graphitic carbon nanomaterials (Li et al., 2010), graphynes, especially GDY, have drawn broad interdisciplinary attention because of their fascinating structures and electronic properties (Li et al., 2014; Zhou et al., 2015). The unique nature of GDY holds great promise for practical applications in batteries, electrics, solar cells, catalysis, detection, and energy storage (Zhou et al., 2015; Zhang et al., 2015; Jia et al., 2017; Kuang et al., 2015; Yang et al., 2013; Li et al., 2017a, 2018c; Gao et al., 2019; Xiao et al., 2015). To date, though, the use of GDY and its derivatives in the field of antibacterial research has not been explored or reported. Because GDY has a natural semiconductor band gap and superior electrical properties (Zheng et al., 2018; Inagaki and Kang, 2014), we postulate that it should be capable of serving as a photocatalytic disinfectant to eliminate harmful bacteria, giving rise to a new class of antibacterial nanomaterials. However, the surface of GDY is highly hydrophobic and chemically inert, limiting its interaction with bacteria in an aqueous system and thereby lessening its antibacterial efficacy. As surface oxidation makes 2D nanomaterials more hydrophilic, we propose a new

[1]College of Chemistry and Chemical Engineering, Inner Mongolia University, 235 University West Street, Hohhot 010021, China

[2]Laboratory of Organic Solids and Beijing National Laboratory for Molecular Sciences, Institute of Chemistry, Chinese Academy of Sciences, No. 2 North First Street, Zhongguancun, Beijing 100190, China

[3]International Joint Research Laboratory of Nano-Micro Architecture Chemistry, College of Chemistry, Jilin University, 2699 Qianjin Street, Changchun 130012, P.R. China

[4]California NanoSystems Institute and Department of Chemistry & Biochemistry, University of California, Los Angeles, CA 90095, USA

[5]Engineering Research Center of Dairy Quality and Safety Control Technology, Ministry of Education,Inner Mongolia University, 235 University West Street, Hohhot 010021, China

[6]Lead Contact

*Correspondence: liyj@iccas.ac.cn (Y.L.), ywyang@jlu.edu.cn (Y.-W.Y.), dongali@imu.edu.cn (A.D.)

https://doi.org/10.1016/j.isci.2019.08.019

strategy using simple surface oxidation, which modifies the surface of GDY to promote its hydrophilicity and improve its antibacterial activity.

In this work, we report for the first time on the antibacterial behaviors of GDY and graphdiyne oxide (GDYO), focusing on their antibacterial performance and bactericidal mechanisms. Using GDY as a starting material, we synthesize GDYO through surface oxidation with H_2O_2/H_2SO_4 as the oxidizing agent, thereby regulating the hydrophilic groups on the GDY surface. To better understand the antibacterial capabilities of GDY and GDYO, we use a series of experiments to explore their antibacterial activity against two models, *Escherichia coli* and *Staphylococcus aureus*. Interestingly, GDYO shows higher antibacterial activity than GDY against both models. We attribute this mainly to ROS-dependent oxidative stress, with the prerequisite that the bacteria have direct contact with a dispersed GDYO suspension. On the basis of these findings, we introduce GDYO as a new family of 2D antibacterial nanomaterials that will hopefully open the door for graphdiyne-based nanomaterials in antibacterial and related applications.

RESULTS AND DISCUSSION

The GDY employed herein was synthesized on the surface of copper via a cross-coupling reaction according to our previously reported procedure (Li et al., 2010). GDY is a 2D network in which the connecting units consist of a six-membered carbon ring in the center and six carbon triple bonds attached to each of the ring's carbon atoms (Ivanovskii, 2013; Huang et al., 2018). The flat carbon networks contain only sp- and sp^2-hybridized carbon atoms with a high π-conjugation (Zhou et al., 2015). As shown in Figure 1A, GDYO was generated by ultrasonic processing on GDY flakes, followed by a modified Hummer's method using a mixture of H_2O_2/H_2SO_4 as the oxidizing agent in an ice-water bath. Transmission electron microscopic images reveal that all three products, i.e., GDY (Figures 1B and S1A), ultrasonicated GDY (Figure S2), and GDYO (Figures 1C and S1B), have a thin, sheet-like morphology with occasional folds. A close-up view confirms that all three products are composed of multilayer nanosheets deposited in a high-density tidy orientation, suggesting that the fabrication process that combines ultrasonication and oxidation could render GDYO a sheet-like morphology. Atomic force microscopic images indicate that GDY (Figures 1D and S3A) and GDYO (Figures 1E and S3B) have a thickness of 4–9 nm and 4–11 nm, respectively, further demonstrating that they are made up of multilayer nanosheets with uniform thickness. Dynamic light scattering results reveal that GDY (Figure 1F) and GDYO (Figure 1G) have narrow size (hydrodynamic size) distributions, and their average lateral sizes are ~410 and ~370 nm, respectively. Interestingly, GDY shows a larger hydrodynamic size than GDYO, confirming that GDYO has better dispersity in an aqueous solution.

To clarify the differences between the chemical compositions of GDY and GDYO, we performed a scanning transmission electron microscopic (STEM)-mapping test, as seen in Figures 2A (GDY), 2B (GDYO), and S4 (ultrasonicated GDY). The element distributions well match with the sheet-like appearance observable in the STEM images. Interestingly, the signal dots of elemental O (red) corresponded well with those of elemental C (green), on behalf of the oxygen envelope on carbon matrixes for all three products. Compared with GDY, GDYO has a higher oxygen density on the surface, indicating the successful surface oxidation of GDY with H_2O_2/H_2SO_4. The presence of carbon and oxygen was further confirmed by the energy-dispersive X-ray spectra (Figure S5), suggesting there are C- and O-containing surface terminations on both GDY and GDYO. A stronger O peak for GDYO than for GDY is also a good evidence of oxidation on the surface of GDY.

Raman spectroscopy and Fourier-transform infrared (FTIR) spectroscopy were also recorded to authenticate the production of GDYO. In Figure 2C, the Raman spectrum of GDY (black curve) presents the D (1,360 cm^{-1}) and G (1,578 cm^{-1}) peaks corresponding to carbon materials, as well as the vibration of acetylenic linkages (C≡C) at around 2,140 cm^{-1} (Xue et al., 2016; Huang et al., 2015b). After surface oxidation, the as-produced GDYO (red curve in Figure 2C) still retains the D (1,407 cm^{-1}) and G (1,578 cm^{-1}) peaks, and the C≡C (2,143 cm^{-1}) peak is strong, suggesting that the C≡C structures were not destroyed during the oxidation treatment with H_2O_2/H_2SO_4. The ratio of the D peak to the G peak is 1.57 for GDY and 1.45 for GDYO, indicating some defects of both GDY and GDYO (Li et al., 2017b; Shi et al., 2018). In Figure 2D, the FTIR spectrum of GDY (black curve) displays three characteristic peaks at 3,423 cm^{-1}, 1,614 cm^{-1}, and 1,266 cm^{-1}, attributable to the -OH stretching vibration, the skeleton vibration of the benzene ring, and the C-O-C stretching vibration, respectively. In addition to these three peaks, the FTIR spectrum of GDYO (red curve) shows a peak for the C=O stretching vibration at 1,723 cm^{-1} (Zheng et al., 2018), further suggesting the successful oxidation of the GDY nanosheet using H_2O_2/H_2SO_4.

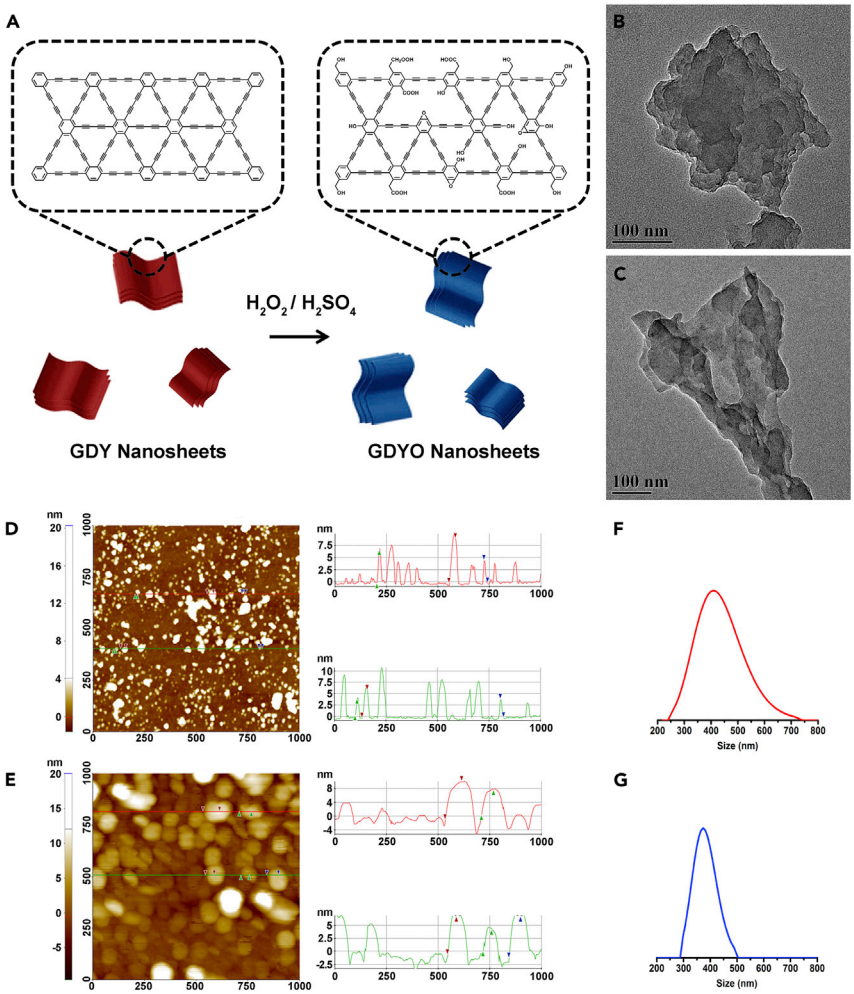

Figure 1. Synthesis and Characterizations of Morphology and Size of GDY and GDYO

(A) Schematic illustration of the synthesis of GDYO nanosheets by surface oxidation on GDY nanosheets.

(B–G) (B and C) Representative transmission electron microscopic image, (D and E) atomic force microscopic image, and (F and G) dynamic light scattering results for GDY (B, D, and F) and GDYO (C, E, and G).

The surface functionalization of GDY via surface oxidation was further confirmed by X-ray photoelectron spectroscopy (XPS) (Figures 2E, 2F, and S6). Figure S6 shows two characteristic peaks corresponding to C 1s and O 1s at 284.8 and 531.2 eV (Zhang et al., 2016; Li et al., 2017c), respectively, for both GDY and GDYO. The intensity of the O 1s signal rises noticeably after GDY has been oxidized by H_2O_2/H_2SO_4, indicating that the oxygen loading is higher on GDYO than on GDY. When the C 1s spectra is deconvoluted (Figures 2E and 2F), both GDY and GDYO show four separate binding energy peaks at 284.5, 285.5, 286.4, and 289.0 eV, corresponding to C-C sp^2, C-C sp, C-O, and C=O, respectively (Li et al., 2016; Jin et al., 2016). Significantly, the intensities of the C-O and C=O peaks in GDYO are higher than those in GDY, indicating more oxygen has been loaded on GDYO than on GDY. The molar percentages (mol %) presented in Table 1 show that those of C-O and C=O in the C 1s peaks increased from 11.21 and 2.79 for GDY to 21.70 and 12.50 for GDYO. Then we measured the zeta potential of GDY and GDYO. As shown in Figure S7, both GDY and GDYO show negative zeta potentials owing to their negatively charged groups on surface, such as -OH, -COOH, C-O-C, etc. Interestingly, GDYO shows a more negative value (-40.89 ± 1.2 mV) than GDY (-35.65 ± 1.0 mV), indicating that GDYO contains more negatively charged groups on surface than GDY.

To the best of our knowledge, the bactericidal effectiveness of graphdiyne-based nanomaterials has not been reported in the literature, although many other carbon nanomaterials, e.g., fullerenes, carbon

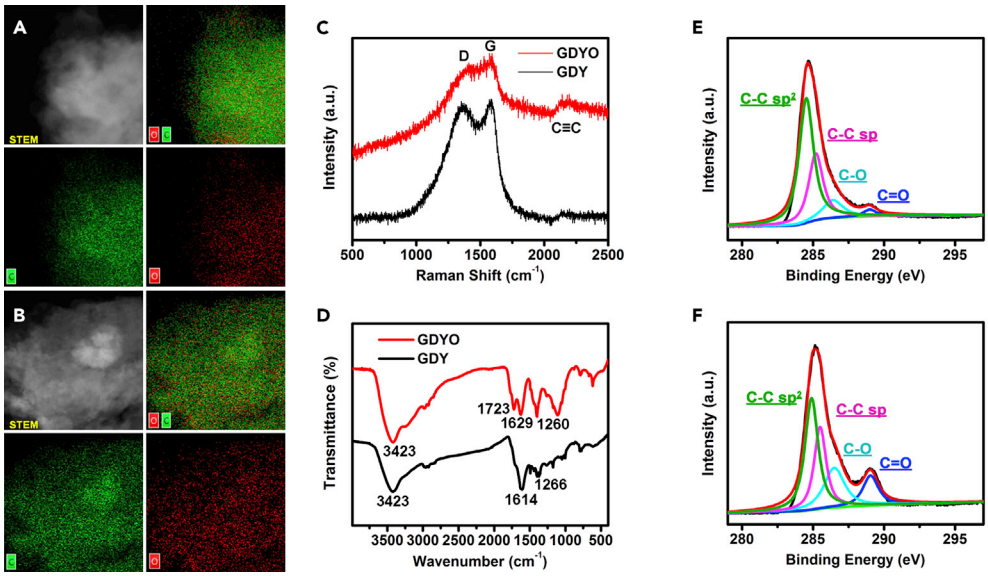

Figure 2. Characterizations of the Chemical Compositions of GDY and GDYO

(A and B) Representative transmission electron microscopic mapping of (A) GDY and (B) GDYO.

(C–F) (C) Raman spectra and (D) FTIR spectra of GDY and GDYO. C 1s peak in the XPS spectra of (E) GDY and (F) GDYO.

nanotubes, and graphene derivatives, have been examined and are regarded as good antibacterial nanomaterials (Li et al., 2015; Xin et al., 2018). For the first time, we investigated the antibacterial activity of GDY and GDYO against representative bacteria, using the colony-counting method. When *E. coli*, a common gram-negative bacteria, was used at a density of 10^5 colony-forming unit (CFU)·mL^{-1} as a representative model of pathogenic bacteria (in Figures 3A and S8A), GDYO displayed antibacterial activity but GDY showed very low or no bactericidal ability. After 120 min of incubation, the survival rate of *E. coli* in the presence of GDYO was 40% in the dark and 2% under visible light irradiation, compared with survival rates exceeding 90% in the presence of GDY, whether in the dark or under visible light irradiation. This difference between GDY and GDYO indicates that surface oxidation grants inert GDY greatly enhanced antibacterial capability, and the increased effectiveness under visible light implies that light has a catalytic effect on the antibacterial action.

The antibacterial property of GDYO was further confirmed by selecting another pathogenic bacteria, *S. aureus*, a common Gram-positive bacteria. We compared the corresponding results to those with *E. coli*. Under visible light irradiation (Figures 3B and S8B), *E. coli* showed 20% survival in the presence of GDYO, compared with no survival by *S. aureus* under the same conditions, confirming that GDYO is more effective against *S. aureus* than against *E. coli* under visible light irradiation. In the dark, a 90% survival rate for *E. coli* versus 0% survival for *S. aureus* further demonstrates the greater inhibition impact of GDYO on *S. aureus*. Generally, whether in the dark or under visible light irradiation, GDYO exhibits stronger antibacterial activity against *S. aureus* than against *E. coli*. The differences in cell structure between Gram-positive and Gram-negative bacteria make *S. aureus* more vulnerable to GDYO than *E. coli* (Wu et al., 2013; Liu et al., 2009).

The above-mentioned examinations confirmed several factors that influence the antibacterial activity of GDYO, i.e., surface oxidation, visible light irradiation, and bacterial species. We then examined the time-dependent antibacterial action of GDYO via an antibacterial kinetic test. Two bacterial strains (10^5 CFU·mL^{-1}) were incubated with GDYO dispersion (3.0 mg·mL^{-1}) for different incubation periods, with GDY as the comparative control. To further confirm the impact of visible light on antibacterial efficiency, the kinetic tests were performed in dark and under visible light. The results with *E. coli* are shown in Figure 3C. The GDYO dispersion exhibited high antibacterial activity both in the dark and under visible light irradiation, whereas the GDY dispersion had almost no bactericidal capacity under either condition during the aging time. Figure 3D presents similar results for *S. aureus* in the presence of GDYO. As can be observed from both panels (Figures 3C and 3D), the survival rate of the two strains significantly decreased as the contact time was extended, indicating the time dependence of GDYO's antibacterial activity.

XPS Peak	Binding Energy (eV)	Mole Percentage (mol %)	
		GDY[a]	GDYO[b]
C-C sp^2	284.5	56.02 ± 8.82	39.50 ± 8.35
C-C sp	285.5	29.98 ± 4.62	26.30 ± 5.02
C-O	286.4	11.21 ± 3.83	21.70 ± 8.18
C=O	289.0	2.79 ± 0.37	12.50 ± 5.20

Table 1. Mole Percentage (mol %) of the Separated Peaks for C 1s in the XPS Spectra of GDY and GDYO

[a]Graphdiyne.

[b]Graphdiyneoxide.

As graphdiyne possesses similar structure to graphene, antibacterial activities of GDY and GDYO were compared with those of graphene (GN, Figures S9A and S9B) and GO (Figures S9C and S9D). Figure 3E shows that owing to their sharp edges that have cutting capability, GN and GO have higher antibacterial activities than GDY and GDYO, whether in the dark or under visible light irradiation. Considering that the interaction of graphdiyne-bacteria examined in saline suspension is not very realistic in any kind of application, antibacterial activities of GDY and GDYO were examined in different media (such as water, NaCl 0.9 wt. %, and $CaCl_2$ 10 mM) and at different pH values (such as 5.3, 7.3, and 9.3). Obviously, GDY and GDYO show similar antibacterial activity in water, NaCl, and $CaCl_2$ solution (Figure 3F), indicating that the addition of Na^+ or Ca^{2+} cannot drive a significant change in the activities of GDY and GDYO. Compared with ion impact, the impact of pH value on antibacterial action of GDY and GDYO is more remarkable. Compared with those at pH 7.3 and pH 5.3, GDY and GDYO endow the highest activity at pH 9.3 (Figure 3G), suggesting that the antibacterial action of GDY and GDYO is pH dependent.

To understand how GDYO deactivates bacteria, we examined bacterial morphology and membrane integrity in the presence of GDYO, using GDY as the comparative material. Figures 4A, 4D, 4G, 4J, and S10 show that bacterial cells incubated with saline solution remained viable and sustained no observable membrane damage or cell death, displaying a smooth and intact surface. Interestingly, observation of GDY-treated bacteria (Figures 4B, 4E, 4H, and 4K) and GDYO-treated bacteria (Figures 4C, 4F, 4I, and 4L) revealed obvious differences between their surfaces. Both *E. coli* and *S. aureus* had relatively smooth surfaces after treatment with GDY, whereas the surfaces of the GDYO-treated bacteria were densely littered with debris, suggesting that GDYO had a destructive effect on the bacteria but GDY did not. We also used STEM-mapping tests to monitor the elemental signals of phosphorus on the bacteria after they were incubated with GDYO; the bacterial cell membrane contains elemental phosphorus, whose distribution might, to some extent, indicate the cell membrane's morphology. The yellow dots in Figure S11 show that the distributions of phosphorus matches well with the corresponding profiles in the STEM images for both *E. coli* and *S. aureus*, further implying the morphological changes induced in the bacteria by GDYO.

Some mechanisms have been proposed to explain the antibacterial action of carbon-based nanomaterials, including oxidative stress, interruption of intracellular metabolic routes, and rupture of cell membranes, of which oxidative stress has been regarded as the most likely mechanism for carbon-based nanomaterials including fullerene, carbon nanotubes, and graphene derivatives (Zou et al., 2016). As GDY is a new class of carbon-based nanomaterials, we speculate that oxidative stress might be responsible for the observed antibacterial behavior of GDYO. It is well known that oxidative stress can follow an ROS-dependent or ROS-independent path (Zou et al., 2016). To clarify which paths are followed in terms of GDY and GDYO, we first examined the generation of ROS in the presence of GDY or GDYO using electron spin resonance (ESR) spectroscopy combined with photometric analysis. In addition, as many carbon-based nanomaterials are capable of producing ROS through visible light-dependent reactions and thereby can cause ROS-dependent oxidative antibacterial effects (Chen et al., 2014b), we also tested ROS generation in the presence or absence of visible light irradiation. When ESR tests were performed (Figure 5), neither GDY nor GDYO produced ROS in the dark, but visible light irradiation induced both to generate four ROS species, i.e., hydroxyl radical •OH, superoxide anion radical $\cdot O_2^-$, and singlet oxygen $^1O_2$, and hydrogen peroxide H_2O_2. We conclude that the production of ROS relies mainly on light irradiation rather than the surface structure of graphdiyne. Next, we also used photometric analysis to study the generation of H_2O_2. Serving similar as pristine H_2O_2 (Figures S12A and S12B), both GDY and GDYO were able to degrade *p*-hydroxyphenylacetic

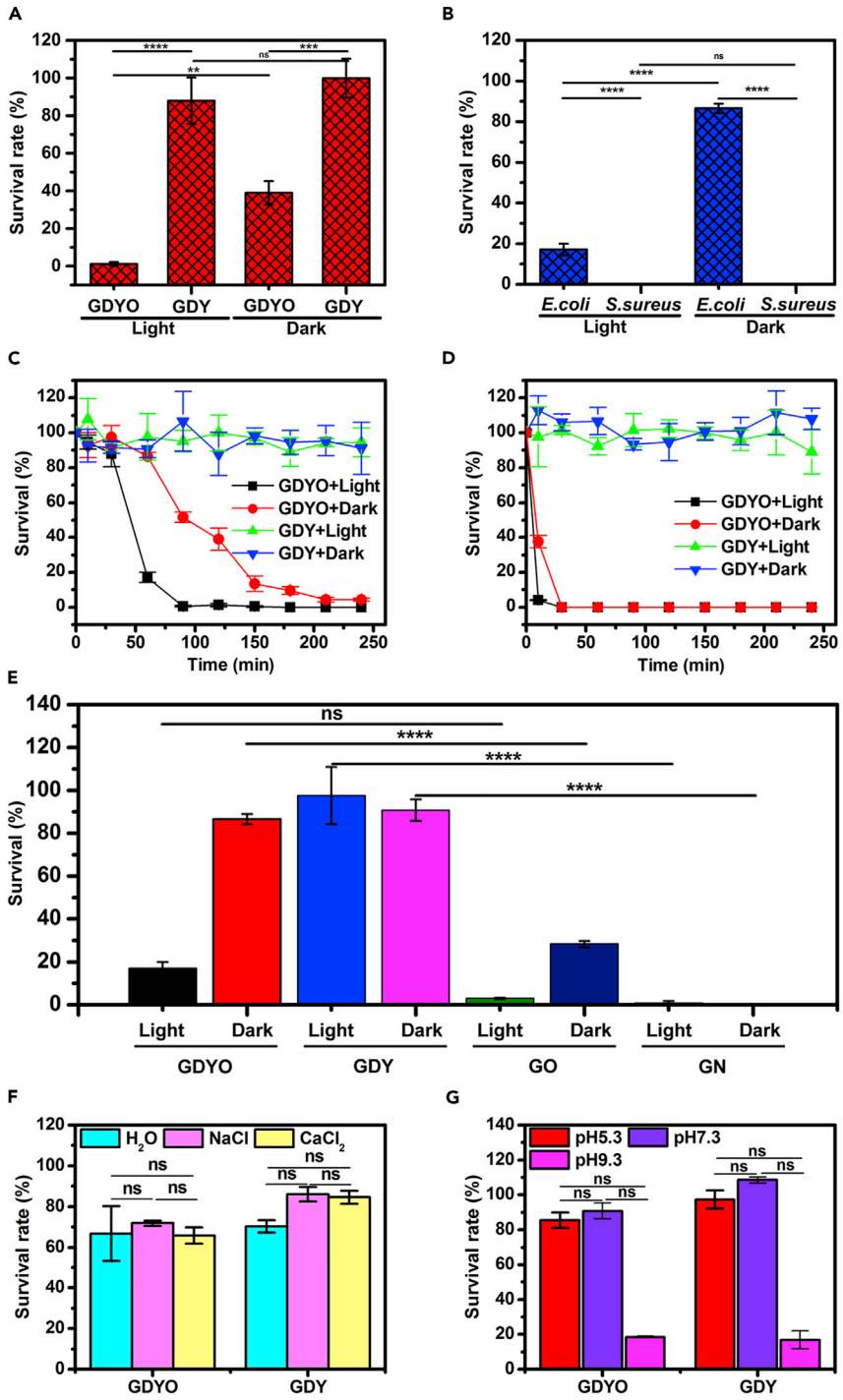

Figure 3. Antibacterial Evaluations of GDY and GDYO

(A) Survival of *E. coli* after treatment with GDY or GDYO for 120 min in the dark and under visible light irradiation.

(B) Survival of *E. coli* and *S. aureus* after treatment with GDYO for 60 min in the dark and under visible light irradiation.

(C and D) Time-dependent antibacterial activity of GDY and GDYO against (C) *E. coli* and (D) *S. aureus* in the dark and under visible light irradiation, respectively.

(E) Survival of *E. coli* after treatment with GDYO, GDY, GO, and GN for 60 min in the dark and under visible light irradiation.

(F and G) Survival of *E. coli* after treatment with GDYO and GDY for 120 min under visible light irradiation (F) in different media and (G) at different pH values.

**p < 0.01, ***p < 0.001, ****p < 0.0001; ns, non-significant (one-way ANOVA).

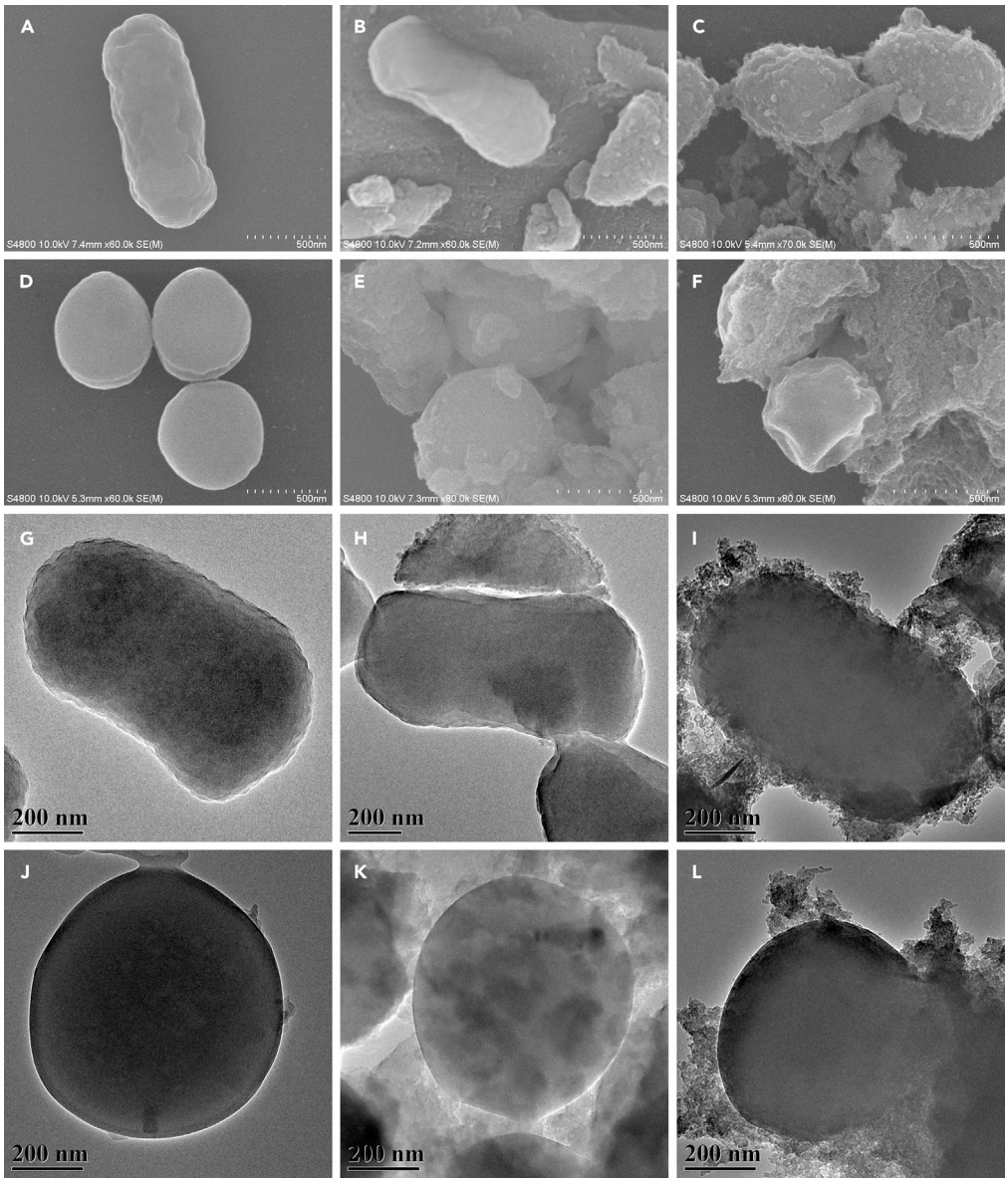

Figure 4. Bacterial Morphology Observation

(A–L) (A–F) Scanning electron microscopic images and (G–L) transmission electron microscopic images of (A–C and G–I) *E. coli* and (D–F and J–L) *S. aureus* after incubation with (A, D, G, and J) saline solution, (B, E, H, and K) GDY suspension, or (C, F, I, and L) GDYO suspension for 4 h under visible light irradiation.

acid under visible light irradiation (Nosaka and Nosaka, 2017), indicating the formation of H_2O_2 in the presence of GDY and GDYO after visible light irradiation. In addition, as shown in Figures 5 and S12C, the generation of ROS is enhanced with both GDY and GDYO when the light exposure time is extended, underscoring the dominant role of visible light irradiation in regulating the generation of ROS, and the time dependence of ROS production.

To understand the active species in the antibacterial process of GDYO, we conducted a scavenging experiment (Chen et al., 2011). using isopropanol alcohol (IPA) to scavenge for •OH (Li et al., 2018d), 4-hydroxy-2,2,6,6-tetramethylpiperidinyloxy (TEMPOL) for $•O_2^-$ (Zhao et al., 2018), sodium azide (NaN_3) for $^1O_2$ (Nosaka and Nosaka, 2017; Wang et al., 2018), and ethylenediaminetetraacetic acid ferric sodium salt (Fe(II)) for H_2O_2 (Zhang et al., 2018). Before the experiment, we made sure that all the scavengers (the

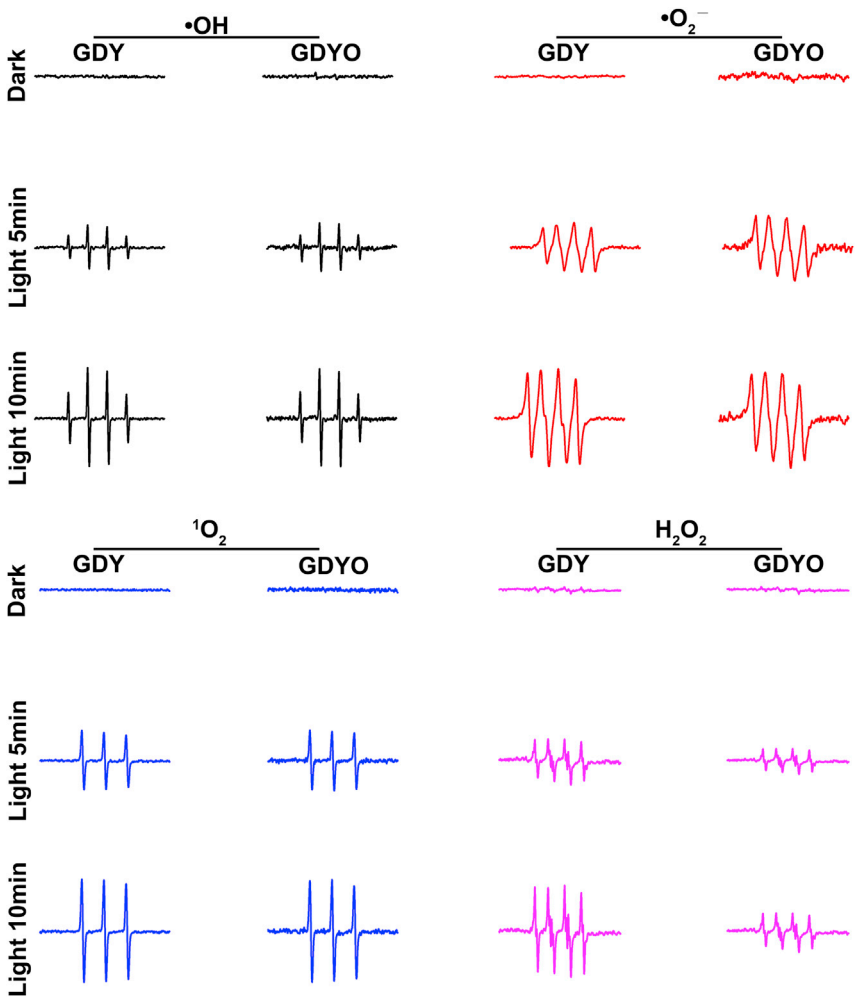

Figure 5. Detection of Reactive Oxygen Species

Electron spin resonance (ESR) spectroscopy of •OH, $•O_2^-$, and $^1O_2$, and H_2O_2, in the presence of GDY and GDYO in the dark and under visible light irradiation.

red curves in Figures 6A–6D) in the concentrations to be used had no (or quite low) bactericidal activity. As shown in Figure 6A, the addition of IPA into the GDYO + Light system scarcely increased bacterial survival, indicating that little •OH is involved in GDYO's antibacterial activity. Bacterial survival increased a bit when TEMPOL (Figure 6B) or Fe (II) (Figure 6D) was added into the GDYO + Light system, demonstrating that $•O_2^-$ and H_2O_2 make a certain contribution to GDYO's antibacterial activity. Interestingly, the GDYO + Light system showed no antibacterial activity in the presence of NaN_3 (Figure 6C), illustrating that $^1O_2$ is the main factor regulating GDYO's antibacterial activity. Hence, in terms of their contribution to GDYO's ROS-dependent antibacterial action (Figure 6E), $^1O_2$ plays a major role, followed by H_2O_2 and $•O_2^-$, and •OH makes the least contribution.

Through the combination of antibacterial results (Figure 3) and ROS analysis (Figure 5), we confirm that GDY has no (or quite low) antibacterial function, whether or not it produces ROS, whereas GDYO kills bacteria in the absence and presence of ROS. Accordingly, we envision that in addition to ROS, GDYO's toxicity toward bacteria may be attributable to a second factor. It has been reported that 2D carbon nanomaterials (e.g., GO nanosheets) can display a blade-like action that destroys the bacterial membrane, presenting a contact-based mechanism (Geng et al., 2017; Akhavan and Ghaderi, 2010). To elucidate the exact role that direct contact plays in GDYO's antibacterial efficiency, we prepared a dried GDYO membrane on the filter (Li et al., 2019), and then *E. coli* suspension was dropped evenly on the

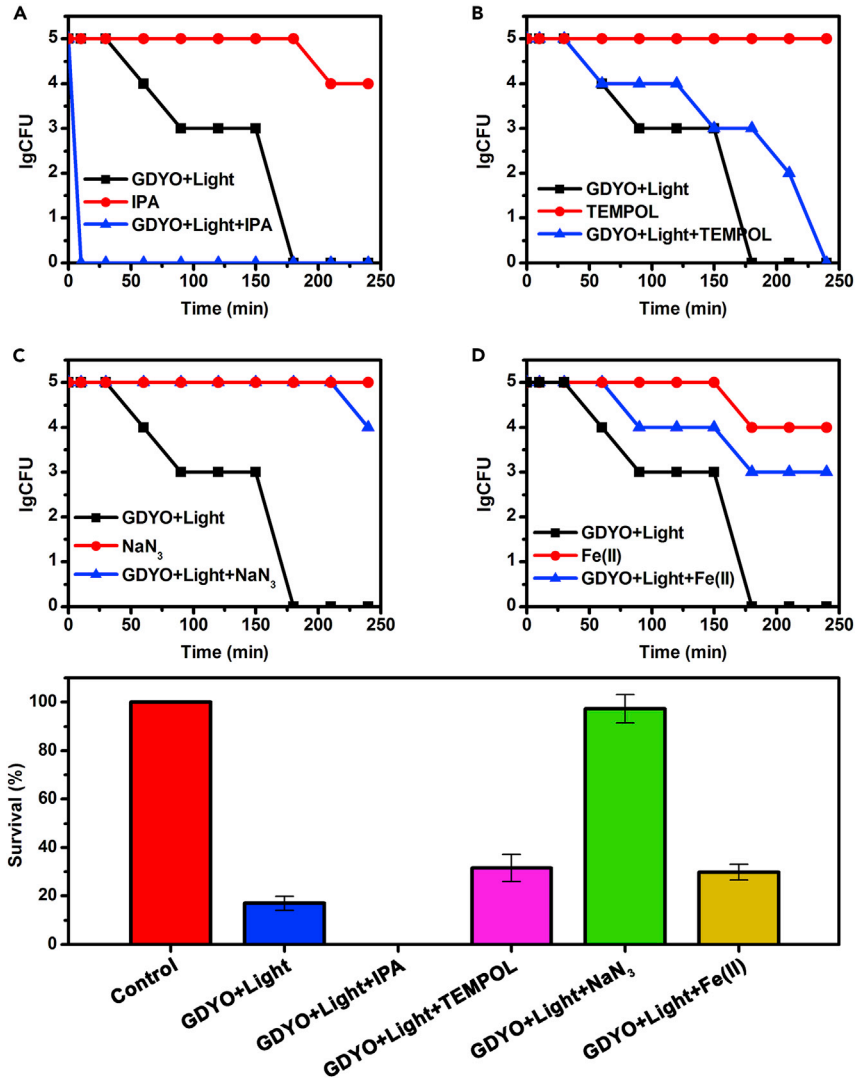

Figure 6. Impact of Reactive Oxygen Species on Antibacterial Efficiency

(A–D) Antibacterial kinetic tests of GDYO against *E. coli* under visible light irradiation in the absence and presence of different scavengers: (A) 0.5 mM of IPA, (B) 2 mM of TEMPOL, (C) 0.077 M of NaN_3, and (D) 2.4 mM of Fe (II). (E) Survival of *E. coli* after incubation with GDYO for 60 min under visible light irradiation in the absence and presence of IPA (0.5 mM), TEMPOL (2 mM), NaN_3 (0.07 M), and Fe (II) (2.4 mM).

surface of GDYO membrane. After a direct contact for 30 min in the dark, *E. coli* on the GDYO membrane was washed with ultrapure water, and the survival of *E. coli* in water was detected using the colony-counting method. As a result, GDYO shows certain bacteria-killing ability by contact (Figure S13), indicating that GDYO possess antibacterial activity even without oxidative stress induced by ROS. Accordingly, one can be sure that GDYO kills bacteria in the dark via the direct contact between bacteria and GDYO.

For antibacterial materials that require contact to be effective, good dispersion in the bacterial suspension is required. So we examined the dispersion behaviors of GDY and GDYO in water. Representative photographs of GDY and GDYO dispersions (concentration: 1.0 $mg \cdot mL^{-1}$) are shown in Figure 7A. Clearly, GDY and GDYO look different because of their distinct structural and physicochemical properties. A black suspension is visible in the GDY dispersion after sonication treatment, and most of the GDY precipitated after standing for $\geq$12 h. The GDYO dispersion obtained by sonication treatment was opaque yellow, and even

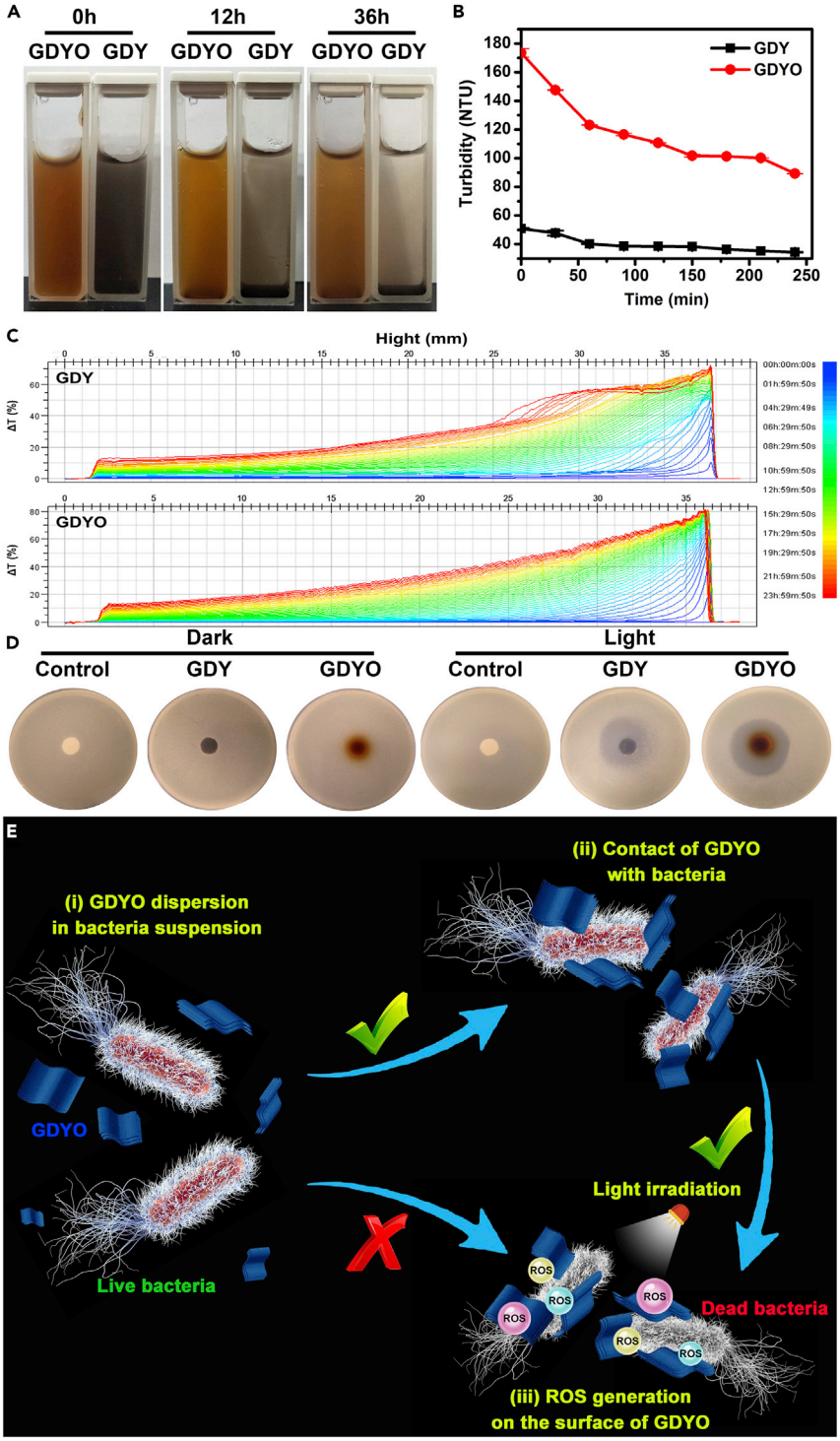

Figure 7. Verification of Antibacterial Mechanism

(A) Photographs of GDY and GDYO dispersions at a concentration of 2.0 mg·mL^{-1} after standing for 0, 12, and 36 h, respectively.

(B) Turbidity of GDY and GDYO dispersion as a function of aging time.

(C) Transmission intensities versus the height of GDY and GDYO in water at different times.

(D) Photographs of inhibition zone assays of GDY and GDYO against *E. coli* in the dark and under visible light irradiation.

(E) A proposed mechanism for the antibacterial action of a GDYO suspension under visible light irradiation.

after standing for 36 h, it remained stable as a homogeneous yellow dispersion with only a small portion of the GDYO precipitating out. Then, turbidity and light scattering of GDY and GDYO dispersion were measured. Figure 7B shows the turbidity of GDY and GDYO as a function of aging time. Obviously, the turbidity of GDYO is higher than that of GDY, demonstrating that GDYO is more stable than GDY in water. We ascribe the good dispersion of GDYO in water to the rich hydrophilic functional groups on the surface of GDYO nanosheets, such as the carboxyl, hydroxyl, and epoxy groups that the FTIR and XPS spectra demonstrated to be present (Figures 2D–2F). The better dispersion of GDYO is consistent with the better antibacterial performance of GDYO compared with GDY (Figure 3), indicating that the higher the dispersion, the more active it will be (Liu et al., 2011). To further understand the dispersion stability of GDY and GDYO, light scattering was performed (Figure 7C). Compared with other carbon materials (Goscianska et al., 2019), GDY and GDYO show high transmission level, indicating that neither GDY nor GDYO is stable enough in static water.

To further confirm the dispersion-dependent antibacterial action of GDYO when it exists in a dispersed form, we then carried out an inhibition zone test in which GDY was employed as the comparative material. As shown in Figure 7D, under visible light irradiation, both GDY and GDYO had inhibition zones with an average diameter of 32.1 and 41.7 mm, respectively, whereas they had no bacteriostatic areas under dark conditions. This is another convincing proof of the importance of visible light irradiation for the antibacterial behavior of GDY and GDYO. With respect to the antibacterial mechanism, the appearance of inhibition zones around GDY and GDYO indicate that at least some of the active components were released from the specimen disk and extended outward, thereby contributing to the antibacterial effect. Such a release-based antibacterial action is especially noticeable from the opaque yellow ring around the GDYO sample under visible light irradiation. When GDY and GDYO are compared, the latter had a larger inhibition zone, which could be explained by GDYO's better dispersion. Strangely, although GDY showed almost no antibacterial activity in the colony-counting test (Figure 3), it showed an obvious inhibition effect under visible light irradiation (Figure 7D). This could be because GDY is more easily exposed to visible light during the inhibition zone test than in the colony-counting test, so its antibacterial behavior can be amplified in the former test.

Based on the above research, GDYO has the following three antibacterial mechanisms: (1) initial good dispersion in the bacterial system, (2) direct contact with the bacteria, and (3) ROS-dependent oxidation stress. Figure 7E presents a diagram of these proposed mechanisms. According to our step-by-step verification of the antibacterial mechanisms, ROS-dependent oxidation stress (especially under visible light irradiation) is the most lethal, but good dispersion and direct contact with the bacteria are prerequisites for the ROS mechanism. We believe that a single antibacterial mechanism may not be sufficient for GDYO to be an effective bactericidal material, and that the three factors affect each other. Owing to its superior antibacterial activity induced by these different mechanisms, GDYO is more potent against the two tested bacteria than GDY, suggesting that surface oxidation grants inert GDY superior antibacterial capability.

Conclusions

We synthesized GDYO from GDY by a simple surface oxidation process, and the subsequent characterizations confirmed that GDYO has a nanosheet-like morphology and abundant carboxyl, hydroxyl, and epoxy functional groups on its surface. Assessment of GDYO's antibacterial activity as an aqueous dispersion showed that it was quite active toward both *E. coli* and *S. aureus*, whereas GDY had little to no antibacterial activity under the same conditions. In addition, the antibacterial activities of GDYO are dependent on visible light, bacterial species, and time. We confirmed that GDYO has a combined antibacterial mechanism that includes dispersion in the bacterial system, direct contact with the bacteria, and ROS-dependent oxidation stress. All these efforts shed light on the bactericidal actions of graphdiyne-based nanomaterials and support their future use in antibacterial applications.

Limitations of Study

Although it is demonstrated that the hydrophilic functional groups on the surface of GDYO nanosheets enable better dispersion in water and allow higher antibacterial efficiency, the relationships between the functional groups and the antibacterial efficiency have not been fully discussed. We believe that further optimizing the functional groups on the surfaces of GDYO nanosheets may further promote the antibacterial activity.

METHODS

All methods can be found in the accompanying Transparent Methods supplemental file.

SUPPLEMENTAL INFORMATION

Supplemental Information can be found online at https://doi.org/10.1016/j.isci.2019.08.019.

ACKNOWLEDGMENTS

This research was supported by the National Natural Science Foundation of China (21304044, 51663019, 21672222, and 21790051), the Natural Science Foundation of Inner Mongolia Autonomous Region (2015MS0520), the State Key Laboratory of Medicinal Chemical Biology (201603006 and 2018051), the State Key Laboratory of Polymer Physics and Chemistry (2018-08), and the Program of Higher-Level Talents of Inner Mongolia University (30105-125136). Y.-W.Y. acknowledges Jilin Province-University Cooperative Construction Project-Special Funds for New Materials (SXGJSF2017-3) and Jilin University Talents Cultivation Program for financial support.

AUTHOR CONTRIBUTIONS

Y.L, Y.-W.Y., A.D., and Y.L. conceived and designed the project. Y.Z. and W.L. performed the experiments under the guidance of Y.L, Y.-W.Y., A.D., and Y.L., including materials synthesis, characterization, antibacterial test, and mechanism verification. All authors discussed the data and commented on the manuscript. Y.Z. and W.L. wrote the paper, and Y.L, Y.-W.Y., A.D., and Y.L. revised the manuscript.

DECLARATION OF INTERESTS

The authors declare no competing financial interests.

Received: March 17, 2019
Revised: July 1, 2019
Accepted: August 12, 2019
Published: September 27, 2019

REFERENCES

Akhavan, O., and Ghaderi, E. (2010). Toxicity of graphene and graphene oxide nanowalls against bacteria. ACS Nano *10*, 5731–5736.

Bunders, C.A., Minvielle, M.J., Worthington, R.J., Ortiz, M., Cavanagh, J., and Melander, C. (2011). Intercepting bacterial indole signaling with flustramine derivatives. J. Am. Chem. Soc. *133*, 20160–20163.

Chambers, H.F., and DeLeo, F.R. (2009). Waves of resistance: *Staphylococcus aureus* in the antibiotic era. Nat. Rev. Microbiol. *7*, 629–641.

Chen, Y., Lu, A., Li, Y., Zhang, L., Yip, H.Y., Zhao, H., An, T., and Wong, P.-K. (2011). Naturally occurring sphalerite as a novel cost-effective photocatalyst for bacterial disinfection under visible light. Environ. Sci. Technol. *45*, 5689–5695.

Chen, J., Peng, H., Wang, X., Shao, F., Yuan, Z., and Han, H. (2014a). Graphene oxide exhibits broad-spectrum antimicrobial activity against bacterial phytopathogens and fungal conidia by intertwining and membrane perturbation. Nanoscale *6*, 1879–1889.

Chen, Z., Li, Z., Wang, J., Ju, E., Zhou, L., Ren, J., and Qu, X. (2014b). A multi-synergistic platform for sequential irradiation-activated high-performance apoptotic cancer therapy. Adv. Funct. Mater. *24*, 522–529.

Djurišić, A.B., Leung, Y.H., and Ng, A.M.C. (2014). Strategies for improving the efficiency of semiconductor metal oxide photocatalysis. Mater. Horiz. *1*, 400–410.

Gao, X., Liu, H., Wang, D., and Zhang, J. (2019). Graphdiyne: synthesis, properties, and applications. Chem. Soc. Rev. *48*, 908–936.

Geng, H., Yao, B., Zhou, J., Liu, K., Bai, G., Li, W., Song, Y., Shi, G., Doi, M., and Wang, J. (2017). Size fractionation of graphene oxide nanosheets via controlled directional freezing. J. Am. Chem. Soc. *139*, 12517–12523.

Goscianska, J., Olejnik, A., and Franus, W. (2019). Multiple light scattering as a method to determine the dispersion stability of amino-functionalized mesoporous carbon. J. Mol. Liquid *278*, 1–4.

Grace, E.S.C., Annamalai, A., Ponmari, G., Vani, C., Rose, A., and Gunasekaran, V. (2015). Cytotoxicity and antibacterial characteristics of graphene-oxide nanosheets toward human pathogens. J. Nanosci. Nanotechnol. *15*, 1–6.

Han, S., Caspers, N., Zaniewski, R.P., Lacey, B.M., Tomaras, A.P., Feng, X., Geoghegan, K.F., and Shanmugasundaram, V. (2011). Distinctive attributes of β-Lactam target proteins in acinetobacter baumannii relevant to development of new antibiotics. J. Am. Chem. Soc. *133*, 20536–20545.

Hegab, H.M., ElMekawy, A., Zou, L., Mulcahy, D., Saint, C.P., and Ginic-Markovic, M. (2016). The controversial antibacterial activity of graphene-based materials. Carbon *105*, 362–376.

Hemeg, H.A. (2017). Nanomaterials for alternative antibacterial therapy. Int. J. Nanomedicine *12*, 8211–8225.

Huang, J.-K., Lauderdale, T.-L.Y., and Shia, K.-S. (2015a). Studies on antibiotics active against resistant bacteria. Total synthesis of MRSA-active tetarimycin A and its analogues. Org. Lett. *17*, 4248–4251.

Huang, C., Zhang, S., Liu, H., Li, Y., Cui, G., and Li, Y. (2015b). Graphdiyne for high capacity and long-life lithium storage. Nano Energy *11*, 481–489.

Huang, C., Li, Y., Wang, N., Xue, Y., Zuo, Z., Liu, H., and Li, Y. (2018). Progress in research into 2D graphdiyne-based materials. Chem. Rev. *118*, 7744–7803.

Inagaki, M., and Kang, F. (2014). Graphene derivatives: graphane, fluorographene, graphene oxide, graphyne and graphdiyne. J. Mater. Chem. A *2*, 13193–13206.

Ivanovskii, I. (2013). Graphynes and graphdyines. Prog. Solid State Chem. *41*, 1–19.

Ji, H., Sun, H., and Qu, X. (2016). Antibacterial applications of graphene-based nanomaterials: recent achievements and challenges. Adv. Drug Deliv. Rev. *105*, 176–189.

Jia, Z., Li, Y., Zuo, Z., Liu, H., Huang, C., and Li, Y. (2017). Synthesis and properties of 2D carbon graphdiyne. Acc. Chem. Res. *50*, 2470–2478.

Jin, Z., Yuan, M., Li, H., Yang, H., Zhou, Q., Liu, H., Lan, X., Liu, M., Wang, J., Sargent, E.H., et al. (2016). Graphdiyne: an efficient hole transporter for stable high-performance colloidal quantum got solar cells. Adv. Funct. Mater. *26*, 5284–5289.

Kuang, C., Tang, G., Jiu, T., Yang, H., Liu, H., Li, B., Luo, W., Li, X., Zhang, W., Lu, F., et al. (2015). Highly efficient electron transport obtained by doping PCBM with graphdiyne in planar-hetero junction perovskite solar cells. Nano Lett. *15*, 2756–2762.

Li, G., Li, Y., Liu, H., Guo, Y., Li, Y., and Zhu, D. (2010). Architecture of graphdiyne nanoscale films. Chem. Commun. (Camb.) *46*, 3256–3258.

Li, Y., Xu, L., Liu, H., and Li, Y. (2014). Graphdiyne and graphyne: from theoretical predictions to practical construction. Chem. Soc. Rev. *43*, 2572–2586.

Li, Z., Liu, Z., Sun, H., and Gao, C. (2015). Superstructured assembly of nanocarbons: fullerenes, nanotubes, and graphene. Chem. Rev. *115*, 7046–7117.

Li, J., Gao, X., Liu, B., Feng, Q., Li, X., Huang, M., Liu, Z., Zhang, J., Tung, C., and Wu, L. (2016). Graphdiyne: a metal-free material as hole transfer layer to fabricate quantum dot-sensitized photocathodes for hydrogen production. J. Am. Chem. Soc. *138*, 3954–3957.

Li, J., Gao, X., Jiang, X., Li, X., Liu, Z., Zhang, J., Tung, C., and Wu, L. (2017a). Graphdiyne: a promising catalyst-support to stabilize cobalt nanoparticles for oxygen evolution. ACS Catal. *7*, 5209–5213.

Li, Y., Guo, C., Li, J., Liao, W., Li, Z., Zhang, J., and Chen, C. (2017b). Pyrolysis-induced synthesis of iron and nitrogen-containing carbon nanolayers modified graphdiyne nanostructure as a promising core-shell electrocatalyst for oxygen reduction reaction. Carbon *119*, 201–210.

Li, S., Chen, Y., Liu, H., Wang, Y., Liu, L., Lv, F., Li, Y., and Wang, S. (2017c). Graphdiyne materials as nanotransducer for in vivo photoacoustic imaging and photothermal therapy of tumor. Chem. Mater. *29*, 6087–6094.

Li, J., Zhang, K., Ruan, L., Chin, S.F., Wickramasinghe, N., Liu, H., Ravikumar, V., Ren, J., Duan, H., Yang, L., et al. (2018a). Block copolymer nanoparticles remove biofilms of drug-resistant gram-Positive Bacteria by nanoscale bacterial debridement. Nano Lett. *18*, 4180–4187.

Li, H., Huang, J., Song, Y., Zhang, M., Wang, H., Lu, F., Huang, H., Liu, Y., Dai, X., Gu, Z., et al. (2018b). Degradable carbon dots with broad-spectrum antibacterial activity. ACS Appl. Mater. Interfaces *10*, 26936–26946.

Li, J., Jiu, J., Chen, S., Liu, L., Yao, Q., Bi, F., Zhao, C., Wang, Z., Zhao, M., Zhang, G., et al. (2018c). Graphdiyne as a host active material for perovskite solar cell application. Nano Lett. *18*, 6941–6947.

Li, C., Sun, Z., Zhang, W., Yu, C., Zheng, S., Li, C., Sun, Z., Zhang, W., Yu, C., and Zheng, S. (2018d). Highly efficient g-C_3N_4/TiO_2/kaolinite composite with novel three-dimensional structure and enhanced visible light responding ability towards ciprofloxacin and *S. aureus*. Appl. Catal. B *220*, 272–282.

Li, P., Li, J., Feng, X., Li, J., Hao, Y., Zhang, J., Wang, H., Yin, A., Zhou, J., Ma, X., and Wang, B. (2019). Metal-organic frameworks with photocatalytic bactericidal activity for integrated air cleaning. Nat. Commun. *10*, 1–10.

Liu, S., Wei, L., Hao, L., Fang, N., Chang, M.W., Xu, R., Yang, Y., and Chen, Y. (2009). Sharper and faster "nanodarts" kill more bacteria: a study of antibacterial activity of individually dispersed pristine single-walled carbon nanotube. ACS Nano *3*, 3891–3902.

Liu, S., Zeng, T., Hofmann, M., Burcombe, E., Wei, J., Jiang, R., Kong, J., and Chen, Y. (2011). Antibacterial activity of graphite, graphite oxide, graphene oxide, and reduced graphene oxide: membrane and oxidative stress. ACS Nano *9*, 6971–6980.

Lu, X., Feng, X., Werber, J.R., Chu, C., Zucker, I., Kim, J.H., Osuji, C.O., and Elimelech, M. (2017). Enhanced antibacterial activity through the controlled alignment of graphene oxide nanosheets. Proc. Nat. Acad. Sci. U S A *114*, 9793–9801.

Nosaka, Y., and Nosaka, A. (2017). Generation and detection of reactive oxygen species in photocatalysis. Chem. Rev. *117*, 11302–11336.

Palmieri, V., Bugli, F., Lauriola, M.C., Cacaci, M., Torelli, R., Ciasca, G., Conti, C., Sanguinetti, M., Papi, M., and Spirito, M.D. (2017a). Bacteria meet graphene: modulation of graphene oxide nanosheet interaction with human pathogens for effective antimicrobial therapy. ACS Biomater. Sci. Eng. *3*, 619–627.

Palmieri, V., Lauriola, M.C., Ciasca, G., Conti, C., Spirito, M.D., and Papi, M. (2017b). The graphene oxide contradictory effects against human pathogens. Nanotechnology *28*, 152001.

Rasool, K., Helal, M., Ali, A., Ren, C.E., Gogotsi, Y., and Mahmoud, K.A. (2016). Antibacterial activity of $Ti_3C_2T_x$ MXene. ACS Nano *10*, 3674–3684.

Rigo, S., Cai, C., Gunkel-Grabole, G., Maurizi, L., Zhang, X., Xu, J., and Palivan, C.G. (2018). Nanoscience-based strategies to engineer antimicrobial surfaces. Adv. Sci. *5*, 1700892.

Rodriguez, R.A., Steed, D.B., Kawamata, Y., Su, S., Smith, P.A., Steed, T.C., Romesberg, F.E., and Baran, P.S. (2014). Axinellamines as broad-spectrum antibacterial agents: scalable synthesis and biology. J. Am. Chem. Soc. *136*, 15403–15413.

Shi, M.-M., Bao, D., Li, S.-J., Wulan, B.-R., Yan, J.-M., and Jiang, Q. (2018). Anchoring PdCu amorphous nanocluster on graphene for electrochemical reduction of N_2 to NH_3 under ambient conditions in aqueous solution. Adv. Energy Mater. *8*, 1800124.

Sikandar, A., Cirnski, K., Testolin, G., Volz, C., Brönstrup, M., Kalinina, O.V., Müller, R., and Koehnke, J. (2018). Adaptation of a bacterial multidrug resistance system revealed by the structure and function of AlbA. J. Am. Chem. Soc. *140*, 16641–16649.

Simpson, L.S., Burdine, L., Dutta, A.K., Feranchak, A.P., and Kodadek, T. (2009). Selective toxin sequestrants for the treatment of bacterial infections. J. Am. Chem. Soc. *131*, 5760–5762.

Tang, S., and Zheng, J. (2018). Antibacterial activity of silver nanoparticles: structural effects. Adv. Healthc. Mater. *7*, 1701503.

Tu, Y., Lv, M., Xiu, P., Huynh, T., Zhang, M., Castelli, M., Liu, Z., Huang, Q., Fan, C., Fang, H., et al. (2013). Destructive extraction of phospholipids from *Escherichia Coli* membranes by graphene nanosheets. Nat. Nanotechnol *8*, 594–601.

Wang, F., Feng, Y., Chen, P., Wang, Y., Su, Y., Zhang, Q., Zeng, Y., Xie, Z., Liu, H., Liu, Y., et al. (2018). Photocatalytic degradation of fluoroquinolone antibiotics using ordered mesoporous g-C_3N_4 under simulated sunlight irradiation: kinetics, mechanism, and antibacterial activity elimination. Appl. Catal. B *227*, 114–122.

Wellington, E.M.H., Boxall, A.B.A., Cross, P., Feil, E.J., Gaze, W.H., Hawkey, P.M., Johnson-Rollings, A.S., Jones, D.L., Lee, N.M., Otten, W., et al. (2013). The role of the natural environment in the emergence of antibiotic resistance in Gram-negative bacteria. Lancet Infect. Dis. *13*, 155–165.

Wu, M., Deokar, A., Liao, J., Shih, P., and Ling, Y. (2013). Graphene-based photothermal agent for rapid and effective killing of bacteria. ACS Nano *7*, 1281–1290.

Xiao, J., Shi, J., Liu, H., Xu, Y., Lv, S., Luo, Y., Li, D., Meng, Q., and Li, Y. (2015). Efficient CH3NH3PbI3 perovskite solar cells based on graphdiyne (GD)-modified P3HT hole-transporting material. Adv. Energy Mater. *5*, 1401943.

Xin, Q., Shah, H., Nawaz, A., Xie, W., Akram, M., Batool, A., Tian, L., Jan, S., Boddula, R., Guo, B., et al. (2018). .Antibacterial carbon-based nanomaterials. Adv. Mater. *30*, 1804838.

Xue, Y., Guo, Y., Yi, Y., Li, Y., Liu, H., Li, D., Yang, W., and Li, Y. (2016). Self-catalyzed growth of Cu@graphdiyne core-shell nanowires array for high efficient hydrogen evolution cathode. Nano Energy *30*, 858–866.

Yang, N., Liu, Y., Wen, H., Tang, Z., Zhao, H., Li, Y., and Wang, D. (2013). Photocatalytic properties of graphdiyne and graphene modified TiO_2: from theory to experiment. ACS Nano *7*, 1504–1512.

Yang, X., Li, J., Liang, T., Ma, C., Zhang, Y., Chen, H., Hanagata, N., Su, H., and Xu, M. (2014). Antibacterial activity of two-dimensional MoS_2 sheets. Nanoscale *6*, 10126–10133.

Zou, X., Zhang, L., Wang, Z., and Luo, Y. (2016). Mechanisms of the antimicrobial activities of graphene materials. J. Am. Chem. Soc. *138*, 2064–2077.

Zhang, S., Liu, H., Huang, C., Cui, G., and Li, Y. (2015). Bulk graphdiyne powder applied for highly efficient lithium storage. Chem. Commun. (Camb.) *51*, 1834–1837.

Zhang, S., Du, H., He, J., Huang, C., Liu, H., Cui, G., and Li, Y. (2016). Nitrogen-doped graphdiyne applied for lithium-ion storage. ACS Appl. Mater. Interfaces *8*, 8467–8473.

Zhang, Y., Lin, C., Lin, Q., Jin, Y., Wang, Y., Zhang, Z., Lina, H., Long, J., and Wang, X. (2018). CuI-BiOI/Cu film for enhanced photo-induced charge separation and visible light antibacterial activity. Appl. Catal. B *235*, 238–245.

Zhao, W., Dai, B., Zhu, F., Tu, X., Xu, J., Zhang, L., Li, S., Dennis, Y., and Cheng, S. (2018). A novel 3D plasmonic p-n heterojunction photocatalyst: Ag nanoparticles on flower-like p-Ag_2S/n-$BiVO_4$ and its excellent photocatalytic reduction and oxidation activities. Appl. Catal. B *229*, 171–180.

Zheng, T., Gao, Y., Deng, X., Liu, H., Liu, J., Liu, R., Shao, J., Li, Y., and Jia, L. (2018). Comparisons between graphene oxide and graphdiyne oxide in physicochemistry biology and cytotoxicity. ACS Appl. Mater. Interfaces *10*, 32946–32954.

Zhou, J., Gao, X., Liu, R., Xie, Z., Yang, J., Zhang, S., Zhang, G., Liu, H., Li, Y., Zhang, J., et al. (2015). Synthesis of graphdiyne nanowalls using acetylenic coupling reaction. J. Am. Chem. Soc. *137*, 7596–7599.

ISCI, Volume *19*

Supplemental Information

2D Graphdiyne Oxide Serves as a Superior New Generation of Antibacterial Agents

Yana Zhang, Wenxin Liu, Yongjun Li, Ying-Wei Yang, Alideertu Dong, and Yuliang Li

Supplemental Information

Transparent Methods

Materials

Concentrated sulfuric acid H_2SO_4, (98 wt %) was supplied by Beijing Chemical Works. Hydrogen peroxide (H_2O_2, 30 wt %) and ethylenediaminetetraacetic acid ferric sodium salt (Fe(II)) were provided by Tianjin Fengchuan Chemical Reagent Technology Co., Ltd. Tert-butanol was obtained from Tianjin Yongda Chemical Reagent Co., Ltd. Glutaraldehyde was provided by Beijing Leagene Biotechnology Co., Ltd. Isopropanol alcohol (IPA) was purchased from Tianjin Fuyu Fine Chemical Co., Ltd. 4-Hydroxy-2,2,6,6-tetramethylpiperidinyloxy (TEMPOL) and *p*-hydroxyphenylacetic acid were supplied by Aladdin Co., Ltd. Sodium azide (NaN_3) was obtained from MRC Co., Ltd. PCX50C Discover as visible light source (420-760 nm). Sodium chloride NaCl was purchased from Tianjin Beilian Fine Chemicals Development Co., Ltd. Distilled water was generated on a Millipore system (Millipore Inc.). Without further purification, all the chemicals were utilized as received. Yeast extract powder was bought from Beijing Aoboxing Biotech Co., Ltd. Beef cream was obtained from Guangdong Huankai Biotech Co., Ltd. Tryptone was purchased from Oxoid Co., Ltd. Agar was provided by Biosharp Co., Ltd. All of the above used in biological tests were biological-reagent grade.

Preparation of GDY and GDYO

GDY was prepared according to the cross-coupling reaction detailed in our previous report (Li et al., 2010). Typically, the monomer of hexaethynylbenzene was synthesized in a yield of 62 % by addition of tetrabutylammonium fluoride (TBAF) to tetrahydrofuran (THF) solution of hexakis[(trimethylsilyl)ethynyl]benzene for 10 min at 8 ^{o}C. The graphdiyne was successfully grown on the surface of copper foil in the presence of pyridine by a cross-coupling reaction of the monomer of hexaethynylbenzene for 72 h at 60 ^{o}C under nitrogen atmosphere. GDYO was synthesized by the simple oxidation of GDY powder using a mixture of H_2O_2 and H_2SO_4 as a complex oxidant. Briefly, 20 mg of GDY was ground for 10 min using an agate mortar, and a GDY dispersion was achieved by the assistance of an ice bath sonication of the GDY powder in 30 mL of distilled water for about 10 hours. Ultrasonicated GDY was obtained by freeze-drying. Subsequently, 20 mg of the ultrasonicated GDY was gradually stirred into 30 wt % H_2O_2 solution (2 mL) and 98 wt % H_2SO_4 (6 mL) under an ice-water bath for 5 h. Finally, GDYO was obtained by ultrasonication for 4 hours, followed by a freeze-drying treatment.

Antibacterial Assay

The antibacterial properties of GDY and GDYO were determined via the colony-counting method using *Escherichia coli* (*E. coli*, 8099 Gram-negative bacteria) and *Staphylococcus aureus* (*S. aureus*, ATCC 6538 Gram-positive bacteria) as the bacterial models. Typically, bacterial strains were expanded in a shaking table with a shaking speed of 220 rpm for 12 hours in a liquid medium at 37 ^{o}C to obtain a strain concentration of 10^8-10^9 CFU·mL^{-1} and were stored at 4 ^{o}C. Prior to the antibacterial tests, 1.0 mL of bacterial culture was centrifuged at ~4000 rpm, the as-centrifuged strains were washed three times with a 0.8 wt % sterile aqueous solution of sodium chloride, then gradually diluted to 10^6 CFU·mL^{-1}. 3 mg of GDY and GDYO were dispersed separately in 900 μL of sterilized distilled water, vortexed, and then sonicated for 30 min. For an antibacterial test, 100 μL of bacterial suspension was added into 900 μL of sample suspension, mixed well, and incubated under constant shaking. At different time intervals, aliquots of the mixture above were gathered and then diluted to 10^2 CFU·mL^{-1} using the sterilized saline solution, and then spread

uniformly on nutrient agar plate and incubated at 37 ^{o}C for 24 h. To evaluate the effect of visible light irradiation on antibacterial efficiency, a visible light simulator—a 300 W Xe lamp filtered through a UV cutoff (k < 420 nm)—was used as the light source during the antibacterial procedure, and the control experiments in the dark were conducted in the same way, minus the light. All the inactivation experiments were performed in triplicate. Survival of bacterial colonies was calculated based on the following equation: % survival = (A/B), where A is the number of surviving colonies of the sample and B is the number of surviving colonies of the control.

Impact of ROS on Antibacterial Efficiency

The roles of •OH, $\bullet O_2^-$, $^1O_2$, and H_2O_2 in the antibacterial process were verified by the active oxygen scavenging experiment. The scavengers used in this study were IPA (0.5 mM) for •OH, TEMPOL (2 mM) for $\bullet O_2^-$, NaN_3 (0.077 M) for $^1O_2$, and Fe (II) (2.4 mM) for H_2O_2. The scavenging experiments were carried out under the same conditions as the antibacterial assay described above.

Detection of H_2O_2

The *p*-hydroxyphenylacetic acid could be degraded by H_2O_2, and so the existence of H_2O_2 could be qualitatively detected using the fluorescence spectrophotometry. In this test, 200 μL of GDY dispersion or GDYO dispersion (3 mg·mL^{-1}) was irradiated with visible light for 4 h, followed by the dilution to 3 mL. After the pH was adjusted to 9, 50 μL of *p*-hydroxyphenylacetic acid was added into the dispersion to measure the fluorescence spectrum. *p*-Hydroxyphenylacetic acid (50 μL) was dissolved in 3 mL of distilled water, and the corresponding fluorescence spectrum was measured as a control. In addition, the fluorescence spectra of *p*-hydroxyphenylacetic acid (50 μL) in the presence of H_2O_2 (200 μL and 2200 μL, respectively) were measured to confirm the degradation of *p*-hydroxyphenylacetic acid by H_2O_2.

Bacterial Morphology Observation

GDYO (10 mg) was dispersed in distilled water (1 mL), sonicated for 5 min, mixed with 10^7 CFU·mL^{-1} of bacterial cells, and then irradiated under visible light for 4 h. The mixture above was centrifuged at 4000 rpm for about 10 min and washed at least three times with PBS solution. After that, 1 mL of glutaraldehyde fixative was added into the mixture, and it was then left to stand for 12 h at 4 ^{o}C. The as-obtained mixture was centrifuged at ~4000 rpm, washed with PBS at least three times, and dehydrated with 20 %, 50 %, 80 % or 100 % ethanol. Afterwards, the mixture was washed twice with *t*-butanol, then dissolved in *t*-butanol and allowed to stand at 4 ^{o}C for more than 30 min. Finally, the morphology of bacteria and their interaction with the samples were characterized using SEM, TEM, and STEM mapping.

Dispersity Evaluation

In this test, the dispersity of GDY and GDYO were evaluated as a function of their standing periods. Briefly, GDY and GDYO dispersions (3 mg·mL^{-1}) were obtained by sonicating GDY and GDYO in deionized water using a bath sonicator at 37 kHz for 5 min. Then the GDY and GDYO dispersions were placed separately in cuvettes, and the corresponding photographs were recorded after the cuvettes had been standing for 12 h and 36 h.

Inhibition Zone Test

3 mg of GDY and GDYO were well dispersed in 1 mL of distilled water using an ice bath sonicator. The as-obtained GDY and GDYO dispersions were evenly dropped and loaded completely onto filter paper. After a bacterial solution of 10^5 CFU·mL^{-1} was evenly spread on the solid medium and dried,

the sample-loaded filter paper was placed on the medium and incubated at 37 ℃ for 12 h in the dark. For the visible light irradiation group, the sample-loaded filter paper was placed on the medium and irradiated under visible light for 4 h, then incubated at 37 ℃ for 12 h. The antibacterial capabilities against *E. coli* were confirmed by measuring the inhibition zones.

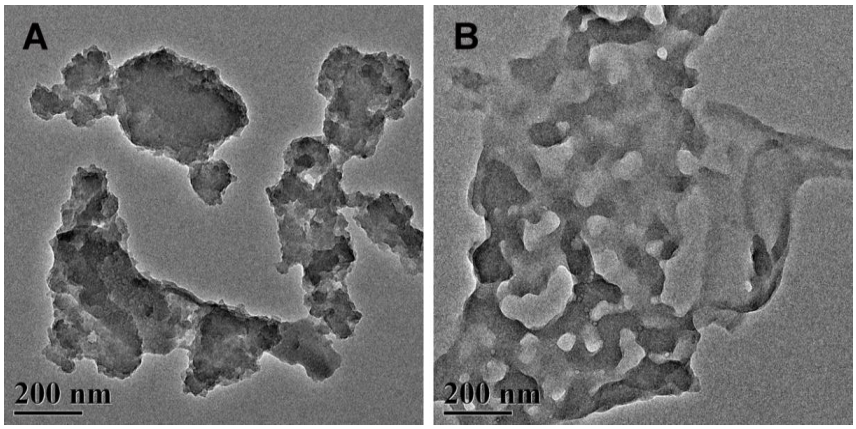

Figure S1. TEM images of (A) GDY and (B) GDYO with low magnification. Related to Figure 1.

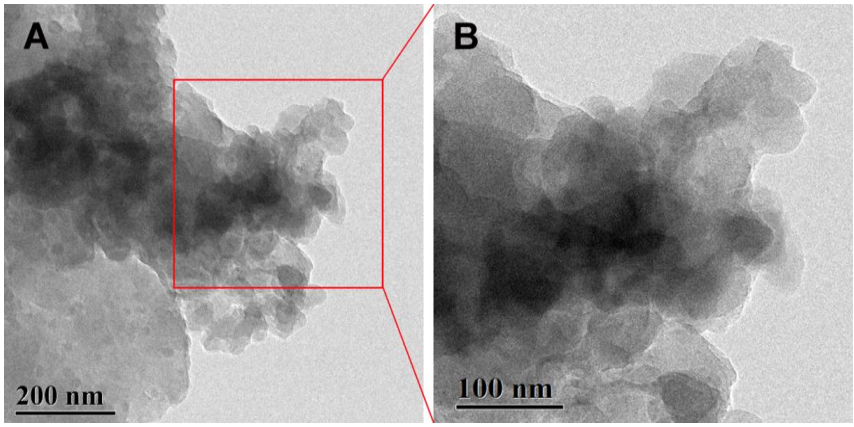

Figure S2. TEM images of ultrasonicated GDY at different magnifications. Related to Figure 1.

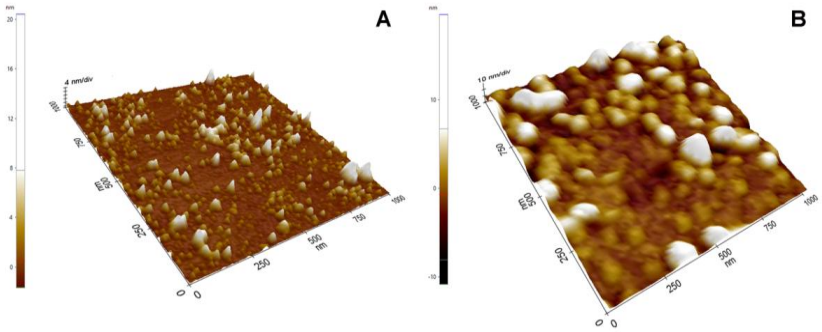

Figure S3. AFM images of (A) GDY and (B) GDYO. Related to Figure 1.

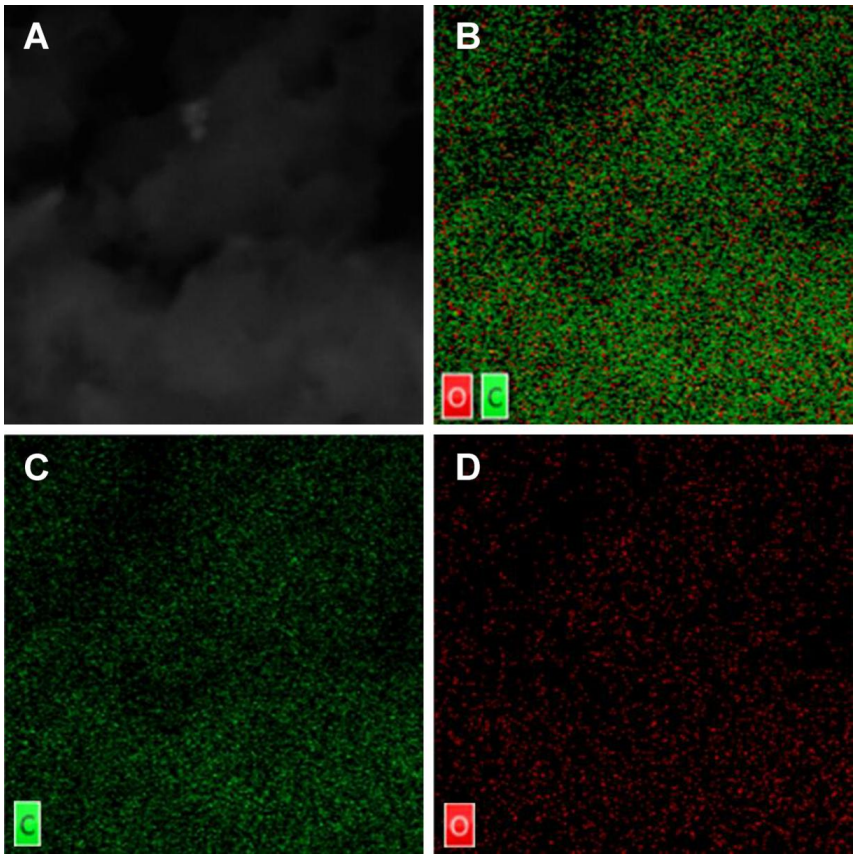

Figure S4. Representative STEM mapping of ultrasonicated GDY. Related to Figure 2.

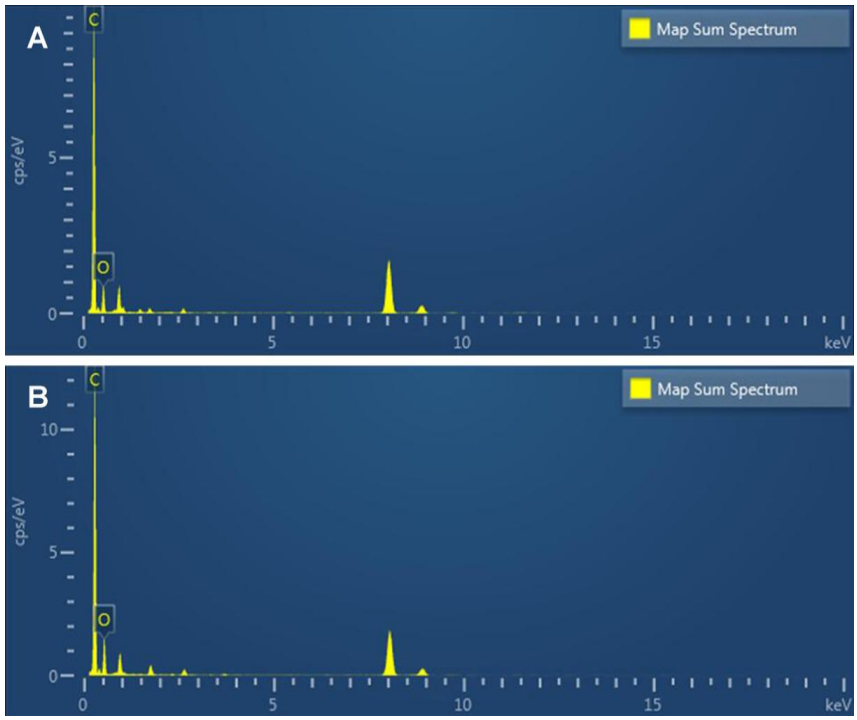

Figure S5. EDX spectra of (A) GDY and (B) GDYO. Related to Figure 2.

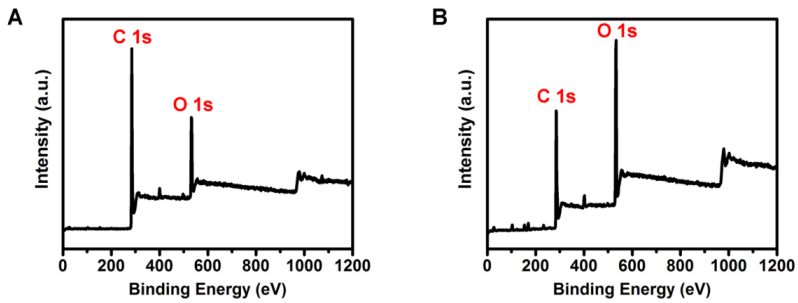

Figure S6. XPS survey spectra of (A) GDY and (B) GDYO. Related to Figure 2.

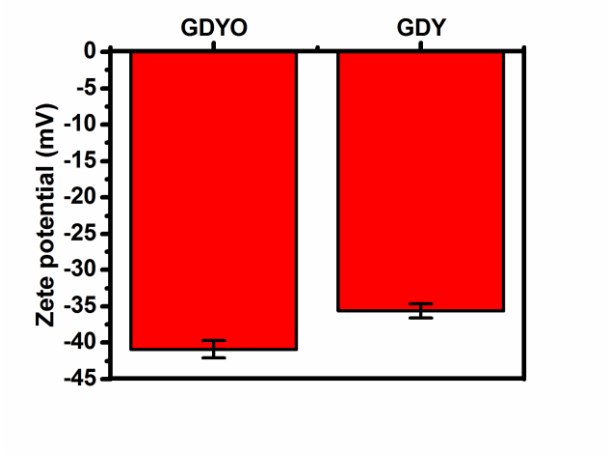

Figure S7. Zeta potentials of GDYO and GDY. Related to Figure 2.

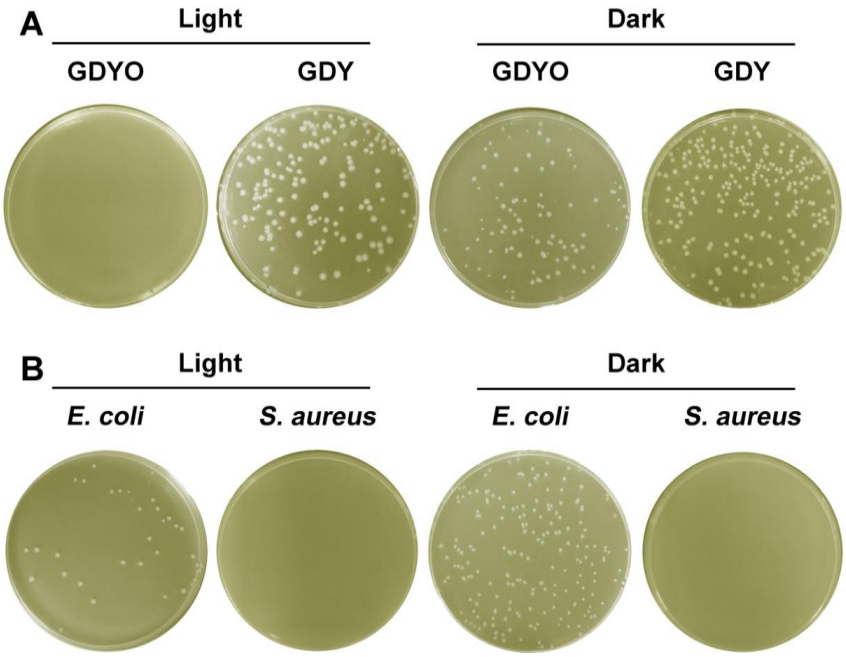

Figure S8. (A) Photographs of the bacterial culture plates of *E. coli* after treatment with GDY or GDYO for 120 min in the dark or under visible light irradiation. (B) Photographs of the bacterial culture plates of *E. coli* and *S. aureus* after treatment with GDYO for 60 min in the dark and under visible light irradiation. Related to Figure 3.

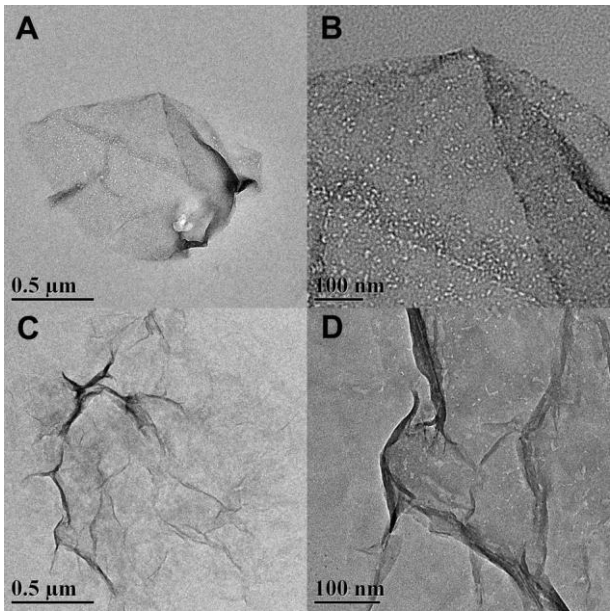

Figure S9. Representative TEM image of GN (A and B) and GO (C and D). Related to Figure 3.

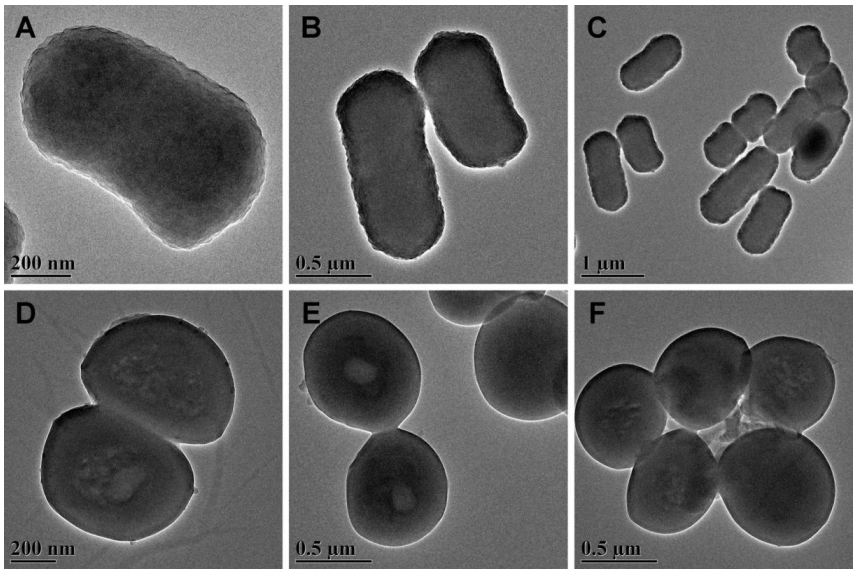

Figure S10. TEM images of (A–C) *E. coli* and (D–F) *S. aureus* after incubation with saline solution. Related to Figure 4.

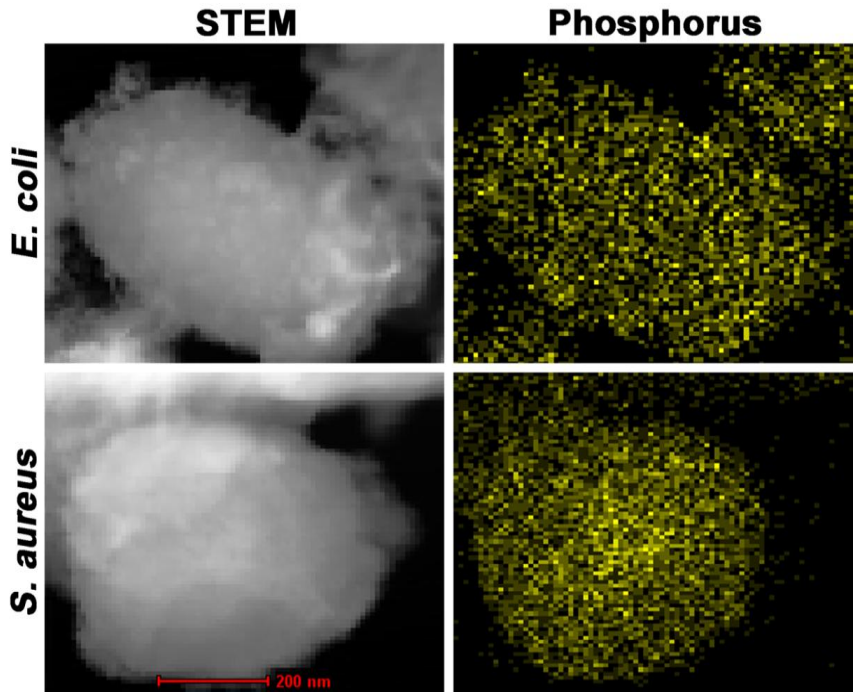

Figure S11. STEM mappings of *E. coli* and *S. aureus* after incubation with GDYO suspension under visible light irradiation for 4 h. Related to Figure 4.

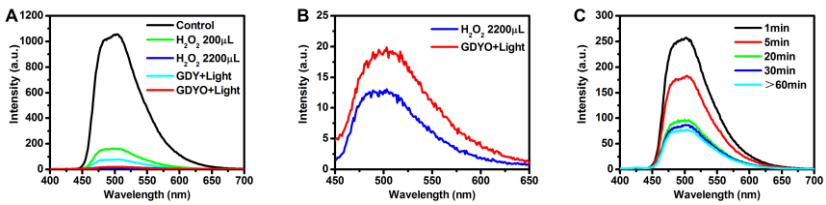

Figure S12. (A and B) The fluorescence spectra of *p*-hydroxyphenylacetic acid in the presence of H_2O_2, GDY and GDYO under visible light irradiation. (C) The fluorescence spectra of *p*-hydroxyphenylacetic acid in the presence of GDYO under visible light irradiation, as a function of aging time. Related to Figure 5.

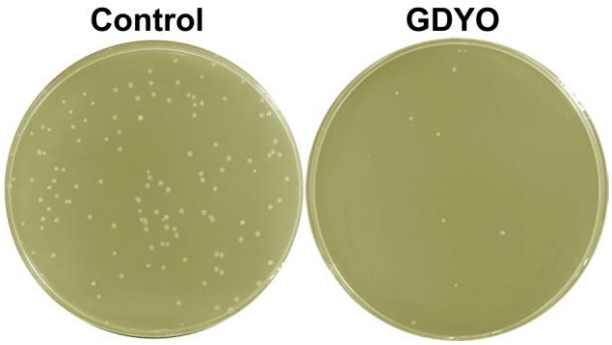

Figure S13. Pictures showing the bacterial survival after direct contact between GDYO with *E. coli*. Related to Figure 7.

Supplemental References

Li, G., Li, Y., Liu, H., Guo, Y., Li, Y., Zhu, D. (2010). Architecture of graphdiyne nanoscale films. Chem. Commun. *46*, 3256-3258.